minerals

MDPI

Article

Biogenic Calcium Carbonate: Phase Conversion in Aqueous Suspensions

Brian Espinosa-Acosta [1], Jake J. Breen [1], Meghan Burchell [2] and Kristin M. Poduska [1,3,*]

[1] Department of Chemistry, Memorial University of Newfoundland & Labrador, St. John's, NL A1C 5S7, Canada; bespinosaaco@mun.ca (B.E.-A.); jjbreen@mun.ca (J.J.B.)
[2] Department of Archaeology, Memorial University of Newfoundland & Labrador, St. John's, NL A1B 3X7, Canada; mburchell@mun.ca
[3] Department of Physics & Physical Oceanography, Memorial University of Newfoundland & Labrador, St. John's, NL A1B 3X7, Canada
* Correspondence: kris@mun.ca

Abstract: Powdered biogenic calcium carbonate from butter clams shows variations in its tendency to convert from aragonite to calcite when suspended in water, depending on whether the suspension has additional calcite or not. Our investigations treat these biogenic samples as complex hierarchical materials, considering both their mineral and organic components. We assess the mineral composition from Attenuated Total Reflection Fourier Transform Infrared spectroscopy peak shifts, as well as quantitative assessments of lattice constant refinements (powder X-ray diffraction). To isolate the mineral portions, we compare results from samples where the periostracum is removed mechanically and samples that are heated to temperatures that are sufficient to remove organic material but well below the temperature for thermal phase conversion from aragonite to calcite. The results show that the total organic content does not play a significant role in the aqueous mineral phase conversion. These results have potential implications for understanding carbonate mineral interactions in ocean sediments.

Keywords: infrared spectroscopy; powder X-ray diffraction; calcium carbonate; aragonite; calcite

Citation: Espinosa-Acosta, B.; Breen, J.J.; Burchell, M.; Poduska, K.M. Biogenic Calcium Carbonate: Phase Conversion in Aqueous Suspensions. *Minerals* **2024**, *14*, 682. https://doi.org/10.3390/min14070682

Academic Editors: Juan Gómez-Barreiro and Natale Perchiazzi

Received: 13 May 2024
Revised: 4 June 2024
Accepted: 25 June 2024
Published: 29 June 2024

1. Introduction

Calcium carbonate ($CaCO_3$), most commonly in the form of calcite or aragonite but also found as vaterite or amorphous calcium carbonate (ACC), is one of the most common biominerals in marine organism skeletons, including clams, oysters, crabs, mussels, and corals [1–3]. Each species has a different predisposition for forming a given polymorph, and it is not uncommon for one species to have different polymorphs in different parts of its hard tissue [4]. For this reason, it is important to acknowledge the individuality of each species when it comes to considering it as a biomaterial.

Between the two most common forms of $CaCO_3$, aragonite is known to have a higher solubility constant than calcite, but both polymorphs have very low solubility in water (aragonite $K_{sp} = 10^{-8.34}$ and calcite $K_{sp} = 10^{-8.48}$ at ambient temperature and pressure [5,6]). Recent studies by us and others [7,8] have demonstrated that this small solubility difference can lead to a surprisingly effective dissolution–recrystallization process in which aragonite can dissolve completely—recrystallizing as calcite—when it is in close proximity to calcite. To describe this in another way, when either calcite or aragonite is present in water on its own, there is only slight solubility. However, when both phases are present, a solution that is in equilibrium with respect to calcite will be undersaturated relative to aragonite, triggering aragonite dissolution; on the other hand, when the solution is in equilibrium with respect to aragonite, it will be supersaturated relative to calcite, which can trigger calcite precipitation. This effect has been effectively modelled based on thermodynamic principles, being described as galvanic dissolution [7], a buffering effect [9], and a thermodynamic

pump [8], since the overall result is to deplete the more soluble phase (aragonite) in favour of the less soluble phase (calcite). Our previous solid-state NMR experiments [8] provided evidence that this is indeed a dissolution–recrystallization process.

Although knowledge of this aragonite-to-calcite conversion process is not new [10,11], the implications of this phase conversion have received more attention recently because of its potential relevance for the stability and preservation of marine minerals. In particular, the time scales and length scales over which this transformation occurs remain open questions, raising the possibility that this process could be important to consider for carbon cycling calculations that involve the ocean. Others have begun exploring these questions through simulations [7], as well as experiments [9,12]. Other more foundational experiments [8] provided evidence that this phase transformation does indeed proceed through a dissolution–recrystallization reaction and that additives to the water (polyphosphate) can become surface-embedded during dissolution–recrystallization, thereby arresting the polymorphic pumping process.

Biogenic calcite and aragonite can have very different microstructures and textures compared to lab-synthesized calcite [13–15]. Bivalves, which are a group of calcium carbonate-shell-forming organisms, produce their shells in layers, where the oldest minerals produced by the organism are found in the inner layer of the shell, and the newest minerals are found in the outer layer of the shell [2,15]. It is well known and documented that bivalves can produce a number of different microstructures of calcite and aragonite through biomineralization and that these possibilities may be different between species. Common microstructures include prismatic, lamellar, and nacreous motifs [3]. The outer and inner layers can have distinct microstructures and will typically vary by species [14]. Thus, an extremely broad range of calcium carbonate microstructures and compositions would exist in any kind of natural environment where powdered aragonite and powdered calcite might interact, such as in sediments.

In this experiment-focused work, we take a simplified model case to consider whether the polymorph composition of biogenic calcium carbonate (calcite, aragonite, or others) is well correlated with the polymorphs that exist when powders of these biomaterials are suspended in freshwater. We use the butter clam as a case study for biogenic calcium carbonate and compare what happens when different portions of the clam—with different pretreatments to remove organic components—are powdered and suspended in ultrapure water. A key aspect of this work is describing polymorph variations that appear in different parts of the clam shell, and unlike some recent work [9], we compare the results with and without the organic components removed. Our data show that some individuals exhibit polymorph behaviour that is similar to what we have observed with lab-synthesized specimens [8,16] and what others have simulated [7] and observed with treated biogenic minerals in treated seawater [9]. We use structural and compositional analyses to assess some of the compositional differences between the lab-synthesized and biogenic materials and to assess under which conditions the biogenic samples exhibit this polymorphic conversion.

2. Materials and Methods

2.1. Overview of Butter Clam Microstructure

Bivalve shells, such as the butter clam, have growth rings that are much like trees, with the relevant layering visible on length scales that are appropriate for optical imaging (tens to hundreds of micrometres) [15]. Figure 1 shows representative views of a half-shell (valve) of the butter clam over different length scales (Zeiss Axiozoom (Oberkochen, Germany) under reflected light, with image enhancement using Adobe Photoshop (version 23, San Jose, CA, USA). The top view of an entire valve (Figure 1a) shows a ridged surface topography, with the axis of maximum growth indicated with a red line. A cross-sectional view along this midline (Figure 1b) shows the growth rings as grey lines. Staining with Mutvei's solution [17] (Figure 1c,d) makes the growth layers easier to see because of the increased visual contrast between the mineral (lower uptake of the stain) and organic-rich

layers in between (higher uptake of stain). The outer proteinaceous layer on the outer surface of the shell (periostracum) also has higher stain uptake.

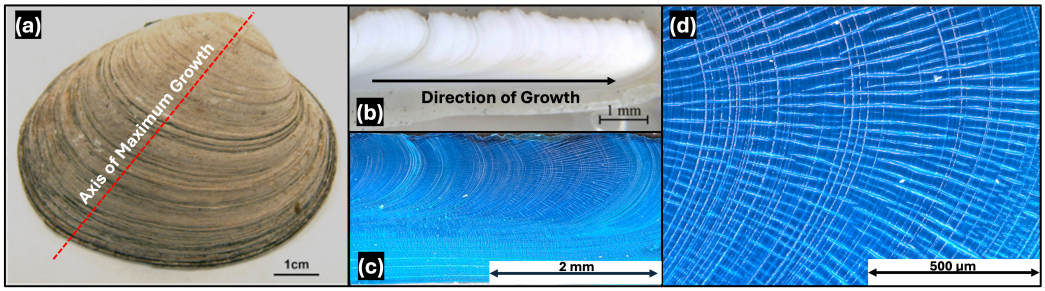

Figure 1. Representative photographs of (**a**) a butter clam valve (midline shown with a red line), (**b**) an unstained section through the valve midline, (**c**) a stained section through the valve midline, and (**d**) a zoom of the stained section through the valve midline. In (**c**,**d**), the organic material is stained darker than the mineral material, which provides better visual contrast for the growth lines.

Even though butter clams are a species of bivalve that is relatively well characterized [18,19], there is still surprisingly little that is known about the specific organic components that exist within the shells. This is an active area of research entailing the characterization of the specific organic proteins and molecules [20]. The mineral portion of butter clam shells has been studied by others. XRD analysis and minor-element composition studies show that butter clam shells are predominantly aragonite [18,19]. The hinge has been more well characterized in the previous literature [21], so we focus our studies on the hinge portions.

2.2. Specimen Preparation

Live-collected, mature (2–6 years old) butter clams (Clams 1 and 2 from Sechelt Inlet, British Columbia, Canada) were sectioned according to Figure 2 and Table 1. The left and right valves were each divided into quarters, yielding four hinge portions and four non-hinge portions per individual. The organic-rich periostracum on the outer portion of the shell was removed mechanically using a hand drill with a 1 mm cylindrical diamond-coated bit (models 27304 and 835104010, Minitor Co., Ltd. (Tokyo, Japan)). Two different half valves (Clams 3 and 4) from dead-collected clams with intact periostracum were also ground and used as separate samples. Butter clams are very hard, and the shells can be crushed and ground only with considerable effort. The most efficient method was hand grinding to a powder (with particle sizes in the range of 40–120 µm) with an agate mortar and pestle; attempts to grind with stainless steel ball milling were abandoned because it introduced metallic debris to the samples.

As outlined in Table 1, selected samples were heated (alumina crucible in a Thermolyne 114,300 furnace) to remove organic material. The heating profile was a ramp from 20 to 300 °C at 100 °C/h, holding at 300 °C for 1 h (except Clam 2 for 3 h), and then cooling to 150 °C before opening the furnace. Table 1 also reports the % mass changes after heating.

Table 1. Labels for different butter clam portions showing their subsequent treatments. Valve and hinge refer to different shell portions shown in Figure 2; a label with "'W" indicates that a whole valve was powdered without sectioning. The organic-rich periostracum was manually removed from some samples before heating; the mass change after heating (ΔMass) is recorded in a separate column. Aqueous suspension experiments used either clam powder alone (clam mass/water volume) or mixtures (clam mass plus purchased calcite mass/water volume), with or without stirring.

Label	Valve	Hinge?	Periostracum?	ΔMass %	Alone (mg:mL)	Mix ((mg):mL)	Stir?
				Clam 1			
1A1	left	yes	yes	–	50:5	(50 + 50):10	yes

Table 1. *Cont.*

Label	Valve	Hinge?	Periostracum?	ΔMass %	Alone (mg:mL)	Mix ((mg):mL)	Stir?
1A2	left	yes	no	–	50:5	(50 + 50):10	yes
1C1	left	no	yes	–	100:10	(50 + 50):10	yes
1B1	right	yes	no	–	10:1	–	yes
			no	−2.9	50:5	(50 + 50):10	yes
1B2	right	yes	yes	–	–	–	yes
			yes	−2.4	50:5	(50 + 50):10	yes
Clam 2							
2B1	right	yes	no	−3.1	–	–	–
2B2	right	yes	yes	−2.6	–	–	–
Clam 3							
3W1	–	–	yes	–	100:10	(50 + 50):10	yes
3W2	–	–	yes	−2.1	100:10	(50 + 50):10	yes
Clam 4							
4W1	–	–	yes	–	–	(50 + 50):10	no
			yes	–	100:10	–	yes

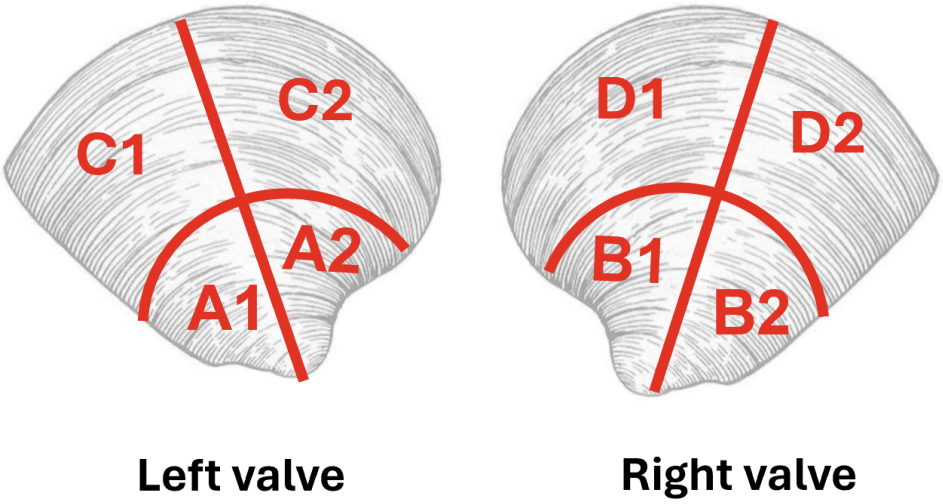

Figure 2. Schematic depiction of the sectioning and labels for different clam portions: A1, A2, B1, and B2 are hinges, while C1, C2, D1, and D2 are non-hinge portions. Adapted from a public domain image [22].

2.3. Aqueous Suspension Experiments

The powders described in Table 1 were tested individually for their polymorph stability in ultrapure water (Barnstead Nanopure, 18.2 MΩ·cm, initial pH 6.7–7.1), with the same mass-to-water ratio for all samples, all in an ambient atmosphere. The powder mass varied among different suspension experiments due to the fact that the different shell portions (Figure 2) did not have the same mass. Suspensions were sonicated for two minutes in capped glass vials and then stirred (Teflon-coated magnetic stir bar, 1000 rpm) for up to 1 week. After 1 week, the supernatants were removed and their pH measured, and the powder was left to dry overnight; the supernatant pH values were 8.3–8.6, which is consistent with trends from earlier studies [23] and is in a similar range to the ambient temperature activity product constants for aragonite (8.36) and calcite (8.52) [24]. We note that, for some heated clam powders, the supernatant pH after one week was slightly higher (9.7). After their suspension, the dried powders were still free-flowing and not densely hard-packed.

In some experiments, after 2 days, 1 mL aliquots of the suspensions were removed by a micropipette and air-dried for further characterization. This allowed us to compare the results of experiments where the vial was opened periodically, exposing the contents to the air, with those where the vials remained capped for the entire experiment. We did not see any differences in the results between these two types of experiments.

A second set of aqueous suspension experiments followed the same procedure described above but involved a mixture of clam powder and purchased calcite. For these experiments, the total proportion of powder to water was the same as above, but the composition of the powder was a 50%–50% mixture by mass of clam powder to purchased calcite (ACS reagent grade, Alfa Aesar, 99%).

2.4. Characterization

Powder X-ray diffraction (PXRD) data for the hand-ground starting powders were collected at room temperature using an XtaLAB Synergy-S, Dualflex, HyPix-6000HE diffractometer (Rigaku, The Woodlands, TX, USA) with Cu Kα radiation (λ = 1.5406 Å). The powder samples were loaded in a 0.5 mm borosilicate glass capillary (HR6-112, Hampton Research). The detector distance was set to 86.0 mm. Data acquisition involved a series of 360 ° ϕ-scans at ω angles of $-65.792°$, $-23.646°$, 23.802°, and 65.948°, with an exposure time of 300 s for each image. Data collection and extraction were performed within CrysAlisPro (version 38, Rigaku OD, Tokyo, Japan, 2024). We refined the lattice constants for each starting material using whole-pattern fitting (JADE 10 software [25]) and compared them with aragonite and calcite unit cells reported in the PDF-2 databases [26]. Additionally, we used Rietveld refinements on selected patterns to assess the phase composition of the starting materials. These results are described in more detail in the Supplementary Materials Table S1 and Figures S1–S5.

To complement the PXRD data, polymorph identification (before and after suspending the powders) was facilitated by Attenuated Total Reflectance Fourier Transform Infrared (ATR-FTIR) spectroscopy (Bruker Alpha with OPUS software version 7.8, Bruker, Billerica, MA, USA), 2 cm^{-1} resolution, 36 scans, 4000–400 cm^{-1} range). Spectra were recorded in triplicate to account for heterogeneity within a given aliquot of powder; a representative subset of these data is shown here, with many dozens of other spectra provided as a dataset. Polymorph assignments were based on comparisons with ATR-FTIR spectral standards (RRUFF project [27]), since the different measurement geometry for transmission FTIR data leads to slightly different peak positions, widths, and asymmetries for the same specimen. We note that Raman spectra are not helpful in these kinds of biogenic samples due to fluorescence interference.

For elemental analysis (Perkin-Elmer 5300 DV ICP-OES (Shelton, CT, USA)), a subset of powders that were used for the PXRD analyses (where there was sufficient mass remaining) were dissolved in acid (HNO_3:HCl 4:1) for 1 h and then diluted to 1%. These solutions were then analyzed for the following elements, which are commonly found in biogenic aragonite: Ca, Mg, Sr, Ba, and Fe.

We assessed the total organic carbon (TOC) data (Shimadzu TOC-L, Kyoto, Japan) before and after heat treatments. The instrument was calibrated with 99% recrystallized acetanilide standards and commercial reference standards from the Hansell consensus reference material program (RSMAS, University of Miami, Coral Gables, FL, USA). Samples were acidified with HCl and then purged with a CO_2-free gas before injection onto a platinum catalyst (at 720 °C). This converted the organic carbon to CO_2 and was quantified by a non-dispersive infrared detector.

3. Results

3.1. Clam Mineral Characterization

Our sample preparation strategy focused on isolating different portions of the clam shell (hinge and non-hinge), followed by different treatments to remove organic material. This gave us several replicates per individual so that we could explore how the mineral part of the shell behaves with and without the periostracum (removed manually), in combination with heating or without heating. We note that our sections give us an average bulk result for a distinct portion of each individual; even so, this sampling strategy glosses over many of the interesting microstructural and textural details of the biogenic specimens

that we described earlier [2,3], but it gives us data that are arguably more representative of what a crushed shell might experience in a natural setting.

Representative ATR-FTIR spectra (Figure 3) show that butter clams are predominantly aragonite, with peaks at 1447–1460 cm^{-1} (ν_3), 1083 cm^{-1} (ν_1), 854–857 cm^{-1} (ν_2), and 712–713 and 700 cm^{-1} (both ν_4). These peak positions are consistent with those reported for aragonite standards, whose spectra were also collected using the ATR-FTIR measurement geometry (RRUFFID = R040078 [27]). There is no evidence of vaterite or amorphous calcium carbonate (ACC), nor is there any difference with or without the periostracum. Additional comparisons among different portions of different shells (listed in Table 1) are shown in Supplementary Materials Figures S6 and S7.

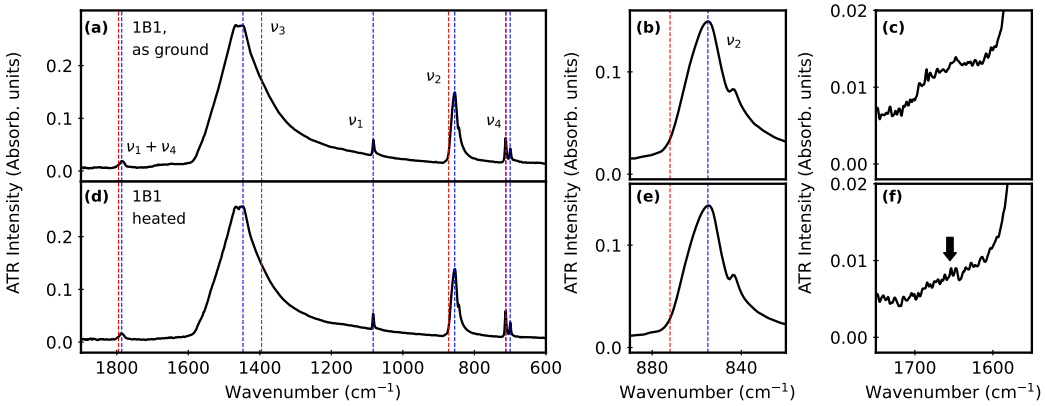

Figure 3. Representative ATR−FTIR spectra for butter clam powder before (**a**–**c**) and after (**d**–**f**) heating. Blue and red vertical lines show peak positions for standards of aragonite (RRUFFID R040078) and calcite (RRUFFID R040070), respectively [27]. Plots (**b**,**e**) focus on the ν_2 region; plots (**c**,**f**) highlight the region where weak protein-based amide and water peaks disappear after heating (1600–1700 cm^{-1}). The black arrow (**f**) highlights the reduction of the protein hump peak intensity after heating.

After heating, ATR-FTIR spectra show a decrease in the broad hump near 1600 cm^{-1} (Figure 3c,f). Since this is a region where amide and water peaks appear [28,29], this kind of change would be consistent with a reduction in protein content. We note that this spectral change is also correlated with a small mass loss (2%–3% in Table 1), which is a similar magnitude of change to that observed after heating other related types of biogenic aragonite (such as Arctica Islandica [30]). The TOC analysis of Clam 3 showed a 60% organic carbon reduction after heating (leaving 0.14% by mass) and a total nitrogen reduction of 60% (leaving <0.02% by mass). Examples of this change in other samples after heating are shown in Supplementary Materials Figure S8.

In PXRD data (Figure 4), we also find that aragonite dominates in all butter clam specimens; Figure 5 summarizes the lattice constant refinement results. Heating decreases the aragonite cell parameters consistently, which is an effect that has been reported by others and is attributed to relaxation and reordering in biogenic aragonite [31,32]. After heating, a new PXRD peak appears (Figure 4b,d) in a region where the strongest calcite diffraction peak (104) would appear. We note that this intensity change is very small, corresponding to less than a few % of the total sample. Additional PXRD spectra are included in Supplementary Materials Figures S10 and S11.

Since we noticed that the aragonite lattice constants for our clams are consistently smaller than the PDF standard, we also looked at elemental analysis data (ICP-OES) for the sample that had enough remaining powder for this measurement (Clam 4). These results show very low amounts of common substitutional impurities that are possible in calcium carbonate (Mg: 0.010(1), Sr: 0.19(3), Fe: 0.007(3), Ba: 0.01(6), all values in wt%). For comparison, the literature data referenced in Figure 5 also have very low impurity

levels. Conch had impurities measured below 0.1 wt% [32], while geogenic aragonite was reported to have atomic wt% of Sr: 0.25, Al: 0.06, Na: 0.03, and Mg: 0.02 [31–33].

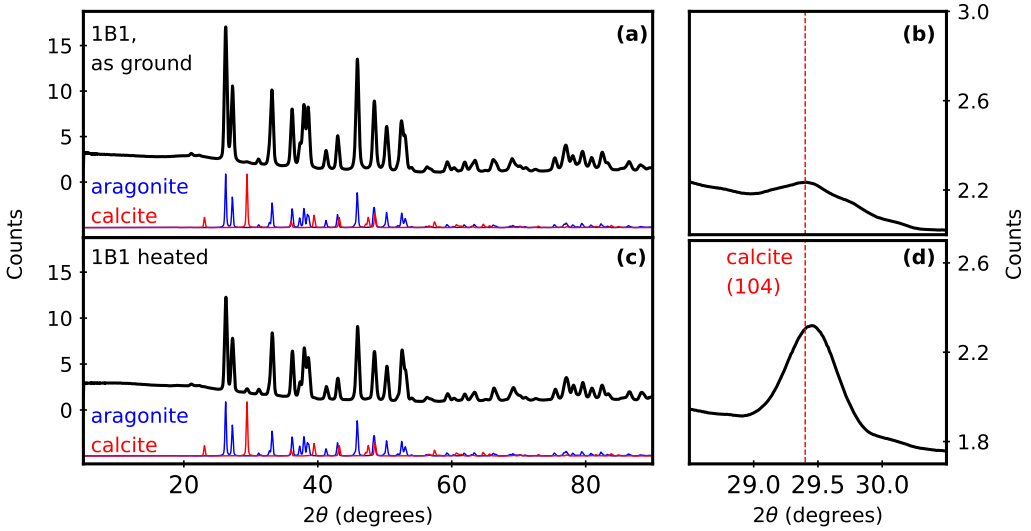

Figure 4. Representative PXRD data of butter clam powder (black lines) before (**a**) and after (**c**) heating. The blue and red patterns show data for standards of aragonite (PDF 980000098) and calcite (PDF 980000141), respectively [26]. Plots (**b**,**d**) show an intensity increase for the strongest calcite line (104) after heating; the dotted red vertical line shows the peak position for the calcite standard pattern.

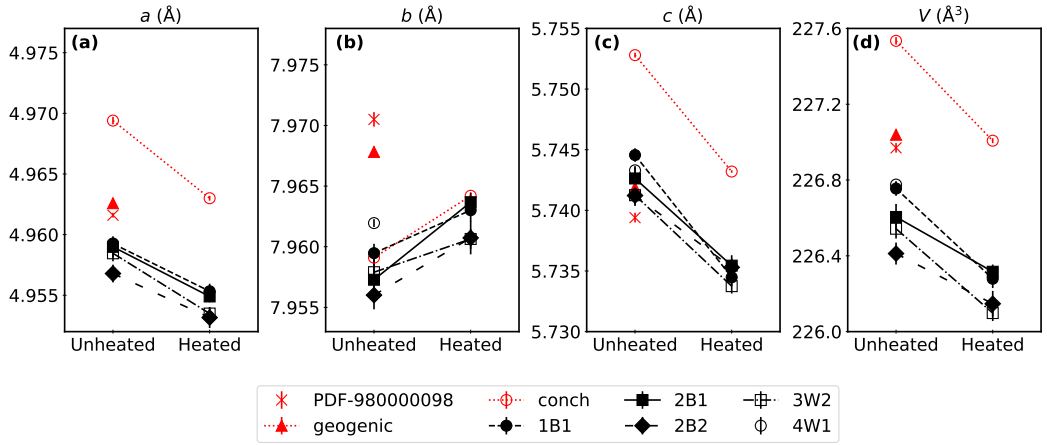

Figure 5. A comparison of aragonite cell parameters a, b, c (in Å) (panels **a**–**c**) and V (volume in Å^3) (panel **d**) , for different clam samples before and after heating (where possible), all shown with black symbols. Red symbols show comparisons to an aragonite standard (PDF# 980000098 [26]) and aragonite parameters reported by others (geogenic and conch from [31–33]).

To summarize, the mineral content of butter clams is predominantly aragonite, with trace amounts of calcite appearing in PXRD data after heating, along with lower-intensity protein-related peaks in ATR-FTIR and some mass loss. We note that leaving the periostracum intact does not lead to any difference in the ATR-FTIR or PXRD data, nor does it change the % mass loss after heating. This suggests that most of the mass loss in these powdered samples is related to either water loss or the elimination of organic material that exists between mineral layers in the shell.

3.2. Monitoring Polymorphs after Aqueous Suspension

In order to track polymorphic phase conversion, we compared the ATR-FTIR spectra of powders before and after they were stirred in water (ultrapure, 18.2 MΩ·cm) for 1 week. A detailed comparison of representative spectra is shown in Figure 6, including a single powder

alone (Figure 6a–d,i–l) or mixtures of clam powder with purchased calcite (Figure 6e–h,m–p). Additional spectra are provided in Supplementary Materials Figures S7 and S9.

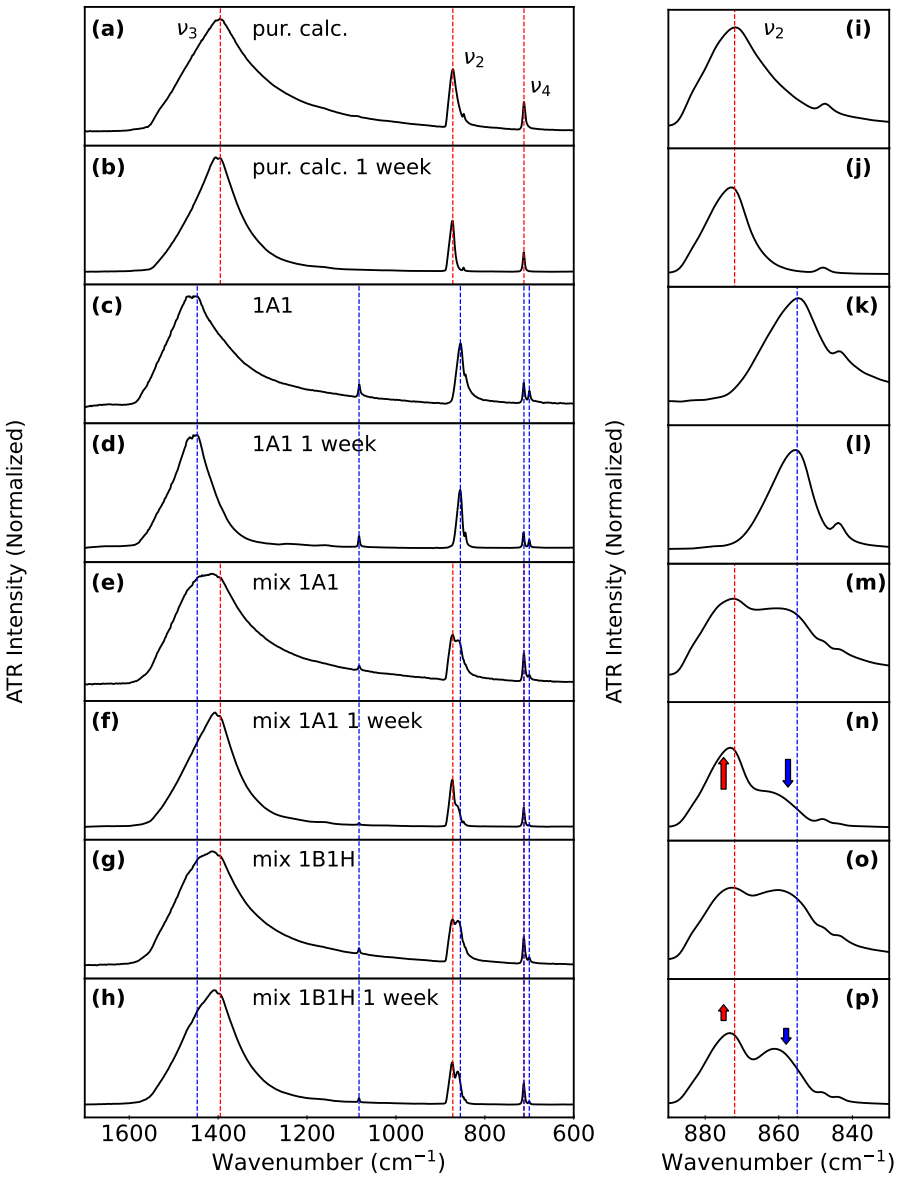

Figure 6. Representative ATR-FTIR spectra to compare changes before and after aqueous suspension. The top 4 rows (**a**–**d**) compare the individual starting materials alone in water; the bottom 4 rows (**e**–**h**) compare mixtures of clam and purchased calcite. Panels (**i**–**p**) show zoomed views of the ν_2 region, where the changes in the relative intensities of the aragonite and calcite peaks are easiest to follow. In all panels, blue and red vertical lines show peak positions for standards of aragonite (RRUFFID R040078) and calcite (RRUFFID R040070), respectively [27]. Arrows highlight the peak intensity changes relative to the pre-suspension spectra for calcite (red) and aragonite (blue).

After stirring clam powder alone in water, there are no distinguishable changes in the ATR-FTIR spectra; in all cases (left/right, hinge/non-hinge, with/without periostracum, with/without heating), aragonite remains the dominant phase, with no clear evidence of conversion to calcite in any case (Figure 6c,d,k,l). However, for sectioned clams that were suspended with purchased calcite (with/without periostracum or with/without heating), some phase conversion from aragonite to calcite is evident in all cases (Figure 6e–h,m–p).

3.3. Biogenic vs. Lab-Synthesized

Since our results show that adding calcite enhances the polymorphic pumping process to make it readily observable in a 1-week time frame, we also investigated other mixed-polymorph scenarios.

For biogenic specimens that already contain mixed polymorphs, the mere co-existence of calcite and aragonite does not guarantee that the polymorphic pumping behaviour is noticeable. Figure 7 helps to illustrate this point. Figure 7a compares ATR-FTIR spectra for heated butter clam powder before and after 1 week of stirring in water. There was no evidence of polymorphic pumping, similar to what is shown in Figure 6c,d,k,l for a different (unheated) clam portion. In both cases, the clam spectra show only aragonite after being stirred in water for one week.

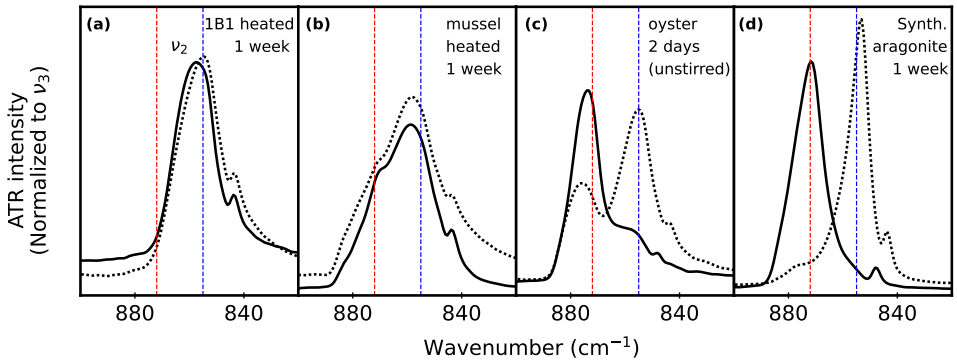

Figure 7. Representative ATR-FTIR spectra comparing polymorphic conversion before (dotted line) and after (solid line) aqueous suspension of (**a**) heated clam powder, (**b**) heated blue mussel powder, (**c**) food-grade oyster shell powder, and (**d**) lab-synthesized aragonite. In all panels, blue and red vertical dashed lines show peak positions for standards of aragonite (RRUFFID R040078) and calcite (RRUFFID R040070), respectively [27].

Blue mussels (Figure 7b) contain a noticeable amount of calcite to start with. For these suspension experiments, a whole ground blue mussel valve (heated in the same way as the clams, with a similar 2.8% mass loss after heating) included both $CaCO_3$ polymorphs in the ν_2 region (Figure 7b), consistent with reports by others [4]. The aragonite and calcite peaks in the ν_2 region do not show any relative intensity changes after 1 week of stirring, whether using heated or unheated powder.

In contrast, we also tested a live-purchased (food-grade) oyster, whose shell consisted of aragonite with calcite as a sizable secondary phase (Figure 7c). For this powdered specimen, it showed significant phase conversion after only 2 days in water, even without stirring.

As another comparison, we were able to observe polymorphic pumping behaviour in lab-synthesized aragonite (Figure 7d), wherein a small amount of calcite was present as an unintentional secondary phase from the synthesis procedure. In this case, 1 week of stirring was enough time for the aragonite to dissolve completely, recrystallizing as calcite. This is consistent with earlier reports from our group [8,16] that confirm this polymorphic pumping behaviour.

To summarize, the tendency toward aragonite dissolution and calcite recrystallization is not the same for all biogenic sources of aragonite and calcite. There are many bivalve species that grow heterogeneous aragonite and calcite distributions within their shells. A polymorph mixture is also possible in specimens in which diagenetic dissolution of aragonite has occurred with reprecipitation as calcite [1]. This means that, even if both aragonite and calcite are present in a specimen, there is no guarantee that polymorphic pumping will happen in similar time frames.

4. Discussion

The polymorph conversion (pumping) that we track in this work relies on two factors: (1) a solubility difference between the two starting polymorphs (calcite and aragonite) and (2) recrystallization that occurs as the less soluble polymorph (calcite) [7,8]. It is a different scenario from direct nucleation from a solution, for which there are many careful studies that document the persistence of multiple $CaCO_3$ polymorphs [13,34]. To this point, our study demonstrates some experiments where polymorphic pumping occurs within a short (1 week) time span and others where the process is much slower.

Since many biominerals are reported to contain substitutional impurities as well as a variety of polymorphs, it is worth commenting on how each of these factors could influence the thermodynamic polymorph pumping behaviour. We also comment on the possible broader relevance to ocean sediment studies.

4.1. Substitutional Impurities

In our samples, we consider lattice constant refinements and elemental analysis information together to assess whether we have evidence for substitutional impurities. Lattice constants and unit cell volumes that are significantly different from those reported for pure $CaCO_3$ could indicate a substitutional impurity: Vegard's law is an empirical linear relation between the unit cell size and substitutional impurity concentration, and it has been usefully applied to many different solid solutions, including $Ca_{1-x}Mg_xCO_3$ [35]. Comparing with representative data for aragonite (Figure 5), we notice that our clam unit cell volumes and *a* value tend to be slightly smaller than the biogenic and geogenic reference values with which we compare. In elemental analyses of the butter clam, the dominant impurity was a very small amount of Sr at 0.19(3) wt%. We note that the elements detected with ICP-OES were not necessarily substitutionally incorporated into the $CaCO_3$ itself. These shells contain a range of macromolecules as a normal part of their structure, some of which would dissolve in the acid dissolution treatment required for the ICP-OES sample preparation.

It is important to note that different apparent solubility constants are not the only way that impurities could influence the dissolution and recrystallization behaviour of aragonite and calcite. Numerous investigations have explored the complex role that the surface incorporation of Sr and Mg, among others, can have on crystal growth rates and surface structures [6,36–39]. Other works show that grain structure and other microstructural factors can yield results that are counter to thermodynamic expectations [40,41]. Earlier work from our group [8,16] shows that polyphosphate can be incorporated into both aragonite and calcite surfaces, which stalls the surface dissolution process for both polymorphs.

4.2. Polymorphism in Bivalves

There are many examples of poorly crystalline carbonates (ACC) in bivalve shells, including oysters [42–44], blue mussels [45,46], and hard clams [42]. Other studies have also shown that ACC, whether biogenic [4] or lab-synthesized [16], can crystallize upon mild heating to temperatures that are far below the temperature at which thermal conversion from aragonite to calcite would occur. This suggests that it should not be surprising that we see weak calcite peaks in our butter clam PXRD data after mild heating, even though ACC has not yet been reported for butter clams.

We note that, even though heating can make a difference in the material composition of our butter clam shells, the resulting loss of organic carbon (assessed through TOC measurements) and the formation of a small amount of calcite (visible in PXRD data) did not accelerate the polymorphic pumping (aragonite-to-calcite) process.

There are many reasons why the biogenic and lab-synthesized samples could have different time scales for observing dissolution and recrystallization behaviours, including the presence of organic molecules or other inorganic material that is incorporated within and between layers of the mineralized specimen. Our experimental design with Clam 1 was intentionally geared toward assessing these variables in a few different ways. The

overall finding was that the mechanical removal of the periostracum did not alter the time scale of the polymorphic conversion in butter clam to any noticeable degree. Using another method to remove organic material, mild heating to a temperature well below where the thermal transition from aragonite to calcite would be expected, did not accelerate the phase conversion: if anything, it appears to have inhibited it slightly.

4.3. Relevance to Ocean Sediment Studies

One context where the time scales for dissolution and crystallization of carbonates are important, but there is much disagreement in the literature, is the long-term stability of biogenic carbonates in ocean sediments [6,47]. This is important not only to understand global carbon budgets [47] but also to recognize that more dissolution-prone ocean-based carbonate producers could be under-represented when considering data based on skeletal material contained in ocean sediments [48]. Earlier studies in freshwater have shown that the dissolution kinetics of biogenic calcite and aragonite are not different from their geogenic counterparts [49]. However, the chemistry of ocean water is significantly more complicated, which has led to more variation in the literature values for carbonate solubilities and dissolution rates [6]. In the specific case that we consider here (aqueous aragonite-to-calcite conversion), there have been recent modelling studies based on different geometric shapes of intact marine organisms [7] that point to the potential relevance of this polymorphic change for modelling geochemistry at the ocean floor.

Exploring more realistic ocean-like conditions in laboratory experiments would include other ions [9,12,38,40] as well as different apparent solubility constants [6,50,51]. The most similar experiment to ours is a recent study [9] that tracked pH in the pore space as a function of time. This elegant study still needed to make some simplifications relative to a true ocean system, including filtered ocean water and the removal of organic material from the shells. Furthermore, while they could detect aragonite dissolution, it was not feasible for them to confirm that there was a concomitant recrystallization of calcite. Thus, that study highlights both the importance—and challenges—of moving toward studies that are more similar to the ocean sediment environment.

5. Conclusions

Our study uses the existing knowledge of microstructural and textural differences among bivalve shells, considering the organic and inorganic portions of such biogenic samples, and follows the behaviour of powdered specimens after suspension in water.

We find the following:

(1) In ultrapure water with stirring, co-suspensions of powdered biogenic bivalves (butter clams or blue mussels) with powdered purchased calcite showed partial aragonite-to-calcite polymorph conversion within a 1-week time frame.
(2) Even small amounts of synthesized calcite in the lab-synthesized aragonite triggered the aragonite-to-calcite phase conversion in ultrapure water; however, the same was not true for small amounts of biogenic calcite in biogenic aragonite under the same conditions.
(3) Heating to remove organics and/or mechanical periostracum removal did not accelerate polymorph conversion (when powdered in an aqueous suspension) within a 1-week time frame.

Our lab-based experiments are one kind of model that makes many simplifications (such as using ultrapure water), but they do respect the complex hierarchical structure of the butter clam by exploring the impact of different portions of the clam shell by comparing results with and without the removal of organic material. They also suggest that different species of bivalves may not undergo phase conversion as rapidly as others, which means that future modelling studies could consider ranges of phase conversion rates, rather than aiming for a single value.

Supplementary Materials: The following are available online at https://www.mdpi.com/article/10.3390/min14070682/s1: Figure S1: Representative diffraction images and corresponding diffraction pattern (2B1); Figure S2: Representative diffraction images and corresponding diffraction pattern (2B1-H); Figure S3: Representative diffraction images and corresponding diffraction pattern (2B2); Figure S4: Representative diffraction images and corresponding diffraction pattern (2B2-H); Figure S5: Representative whole pattern fit for PXRD data from an intentional mixture; Figure S6: Additional ATR-FTIR spectra compared with standards; Figure S7: Additional ATR-FTIR spectra showing starting materials; Figure S8: Additional ATR-FTIR spectra highlighting the aragonite and amine regions; Figure S9: Additional ATR-FTIR spectra showing mixtures before and after aqueous suspension; Figure S10: Additional PXRD data compared with standards; Figure S11: Additional PXRD data showing a weak calcite peak in heated samples; Table S1: PXRD Rietveld refinement results.

Author Contributions: Conceptualization, methodology, and writing—original draft preparation: B.E.-A. and K.M.P.; investigation and data curation: B.E.-A., J.J.B., and M.B.; review and editing: B.E.A., J.J.B., M.B., and K.M.P.; supervision, project administration, and funding acquisition: K.M.P. All authors have read and agreed to the published version of the manuscript.

Funding: This research was funded by the Natural Science and Engineering Research Council of Canada (NSERC), grant number 2018-04888.

Data Availability Statement: The data presented in this study are available at https://doi.org/10.5683/SP3/7UXHRF https://borealisdata.ca/privateurl.xhtml?token=6184caee-d444-4b77-aee3-6dae53ac2957.

Acknowledgments: The authors acknowledge J.B. Lin (X-ray diffraction and Rietveld refinements) and S. Kommescher (ICP-OES) at the Centre for Chemical Research and Training through Memorial University's CREAIT network for access to characterization facilities; K. Heerah and H. Reader, Memorial University Chemistry, for total organic carbon analysis; and Tsleil Waututh Nation for specimen procurement: live-collected butter clams.

Conflicts of Interest: The authors declare no conflicts of interest. The funders had no role in the design of the study; in the collection, analyses, or interpretation of data; in the writing of the manuscript; or in the decision to publish the results.

References

1. Morse, J.W.; Arvidson, R.S.; Lüttge, A. Calcium Carbonate Formation and Dissolution. *Chem. Rev.* **2007**, *107*, 342–381. [CrossRef] [PubMed]
2. Jacob, D.; Soldati, A.; Wirth, R.; Huth, J.; Wehrmeister, U.; Hofmeister, W. Nanostructure, composition and mechanisms of bivalve shell growth. *Geochim. Cosmochim. Acta* **2008**, *72*, 5401–5415. [CrossRef]
3. de Paula, S.M.; Silveira, M. Studies on molluscan shells: Contributions from microscopic and analytical methods. *Micron* **2009**, *40*, 669–690. [CrossRef]
4. Murphy, J.N.; Schneider, C.M.; Mailänder, L.K.; Lepillet, Q.; Hawboldt, K.; Kerton, F.M. Wealth from waste: Blue mussels (*Mylitus edulis*) offer up a sustainable source of natural and synthetic nacre. *Green Chem.* **2019**, *21*, 3920–3929. [CrossRef]
5. Plummer, L.N.; Busenberg, E. The solubilities of calcite, aragonite and vaterite in CO_2-H_2O solutions between 0 and 90 °C, and an evaluation of the aqueous model for the system $CaCO_3$-CO_2-H_2O. *Geochim. Cosmochim. Acta* **1982**, *46*, 1011–1040. [CrossRef]
6. Adkins, J.F.; Naviaux, J.D.; Subhas, A.V.; Dong, S.; Berelson, W.M. The dissolution rate of $CaCO_3$ in the ocean. *Annu. Rev. Mar. Sci.* **2021**, *13*, 57–80. [CrossRef]
7. Sulpis, O.; Agrawal, P.; Wolthers, M.; Munhoven, G.; Walker, M.; Middleburg, J.J. Aragonite dissolution protects calcite at the seafloor. *Nat. Commun.* **2022**, *13*, 1104. [CrossRef] [PubMed]
8. Gao, B.; Kababya, S.; Poduska, K.M.; Schmidt, A. Surface passivation by embedment of polyphosphate inhibits the aragonite-to-calcite thermodynamic pump. *J. Am. Chem. Soc.* **2023**, *145*, 25938–25941. [CrossRef]
9. van de Mortel, H.; Delaigue, L.; Humphreys, M.P.; Middelburg, J.J.; Ossebaar, S.; Bakker, K.; Alexandre, J.P.T.; van Leeuwen-Tolboom, A.W.E.; Wolthers, M.; Sulpis, O. Laboratory observation of the buffering effect of aragonite dissolution at the seafloor. *J. Geophys. Res. Biogeosci.* **2024**, *129*, e2023JG007581. [CrossRef]
10. Yoshioka, S.; Ohde, S.; Kitano, Y.; Kanamori, N. Behaviour of Magnesium and Strontium During the Transformation of Coral Aragonite to Calcite in Aquatic Environments. *Mar. Chem.* **1986**, *18*, 35–48. [CrossRef]
11. Krauskopf, K.B.; Bird, D.K. Solution-Mineral equilibria Part 1: Carbonates. *Introd. Geochem.* **1995**, *3*, 61–83.
12. Sulpis, O.; Lix, C.; Mucci, A.; Boudreau, B.P. Calcite dissolution kinetics at the sediment-water interface in natural seawater. *Mar. Chem.* **2017**, *195*, 70–83. [CrossRef]

13. Zhang, G.; Morales, J.; García-Ruiz, J.M. Growth behaviour of silica/carbonate nanocrystalline composites of calcite and aragonite. *J. Mater. Chem. B* **2017**, *5*, 1658–1663. [CrossRef]
14. Triunfo, C.; Gärtner, S.; Marchini, C.; Fermani, S.; Maoloni, G.; Goffredo, S.; Morales, J.G.; Cölfen, H.; Falini, G. Recovering and Exploiting Aragonite and Calcite Single Crystals with Biologically Controlled Shapes from Mussel Shells. *ACS Omega* **2022**, *7*, 43992–43999. [CrossRef]
15. Louis, V.; Besseau, L.; Lartaud, F. Step in Time: Biomineralisation of Bivalve's Shell. *Front. Mar. Sci.* **2022**, *9*, 906085. [CrossRef]
16. Gao, B.; Poduska, K.M. Comparing Polyphosphate and Orthophosphate Treatments of Solution-Precipitated Aragonite Powders. *Solids* **2022**, *3*, 684–696. [CrossRef]
17. Schöne, B.R.; Dunca, E.; Fiebig, J.; Pfeiffer, M. Mutvei's solution: An ideal agent for resolving microgrowth structures of biogenic carbonates. *Palaeogeogr. Palaeoclimatol. Palaeoecol.* **2005**, *228*, 149–166. [CrossRef]
18. Gillikin, D.P.; Lorrain, A.; Navez, J.; Taylor, J.W.; André, L.; Keppens, E.; Baeyens, W.; Dehairs, F. Strong biological controls on Sr/Ca ratios in aragonitic marine bivalve shells. *Geochem. Geophys. Geosystems* **2005**, *6*, Q05009. [CrossRef]
19. Ulens, H. The Potentials of Saxidomus Giganteus as a Paleoclimate Proxy. Master's Thesis, Gent University, Flanders, Belgium, 2003.
20. Huang, Q.; Wu, H.; Schöne, B.R. A novel trophic archive: Practical considerations of compound-specific amino acid δ^{15}N analysis of carbonate-bound organic matter in bivalve shells (*Arctica islandica*). *Chem. Geol.* **2023**, *615*, 121220. [CrossRef]
21. Hallmann, N.; Burchell, M.; Schöne, B.R.; Irvine, G.V.; Maxwell, D. High-resolution sclerochronological analysis of the bivalve mollusk *Saxidomus gigantea* from Alaska and British Columbia: Techniques for revealing environmental archives and archaeological seasonality. *J. Archaeol. Sci.* **2009**, *36*, 2353–2364. [CrossRef]
22. Available online: https://commons.wikimedia.org/wiki/File:Clam_(PSF).jpg (accessed on 21 March 2024).
23. Gao, B.; Poduska, K.M. Tracking Amorphous Calcium Carbonate Crystallization Products with Far-Infrared Spectroscopy. *Minerals* **2023**, *13*, 110. [CrossRef]
24. Christ, C.L.; Hostetler, P.B.; Siebert, R.M. Stabilities of calcite and aragonite. *J. Geophys. Res.* **1974**, *2*, 175–184. [CrossRef]
25. *JADE 10*; Materials Data: Livermore, CA, USA, 2019.
26. Gates-Rector, S.; Blanton, T. The powder diffraction file: A quality materials characterization database. *Powder Diffr.* **2019**, *34*, 352–360. [CrossRef]
27. Lafuente, B.; Downs, R.T.; Yang, H.; Stone, N.; Armbruster, T.; Danisi, R.M. The power of databases: The RRUFF project. *Highlights Mineral. Crystallogr.* **2015**, *1*, 25.
28. Yang, H.; Yang, S.; Kong, J.; Dong, A.; Yu, S. Obtaining information about protein secondary structures in aqueous solution using Fourier transform IR spectroscopy. *Nat. Protoc.* **2015**, *10*, 382–396. [CrossRef]
29. Kimmel Center for Archaeological Science (Weizmann Institute of Science). Infrared Standards Library. 2021. Available online: https://centers.weizmann.ac.il/kimmel-arch/infrared-spectra-library (accessed on 24 June 2024).
30. Forjanes, P.; Roda, M.S.; Greiner, M.; Griesshaber, E.; Lagos, N.A.; Veintemillas-Verdaguer, S.; Astilleros, J.M.; Fernández-Díaz, L.; Schmahl, W.W. Long-term experimental diagenesis of aragonitic biocarbonates: From organic matter loss to abiogenic calcite formation. *Biogeosci. Discuss* **2021**, *2021*, 1–53. [CrossRef]
31. Pokroy, B.; Fitch, A.; Zolotoyabko, E. Structure of biogenic aragonite ($CaCO_3$). *Cryst. Growth Des.* **2007**, *7*, 1580–1583. [CrossRef]
32. Pokroy, B.; Fieramosca, J.; Von Dreele, R.; Fitch, A.; Caspi, E.; Zolotoyabko, E. Atomic structure of biogenic aragonite. *Chem. Mater.* **2007**, *19*, 3244–3251. [CrossRef]
33. Caspi, E.N.; Pokroy, B.; Lee, P.; Quintana, J.; Zolotoyabko, E. On the structure of aragonite. *Acta Crystallogr. Sect. B Struct. Sci.* **2005**, *61*, 129–132. [CrossRef]
34. Sun, W.; Jayaraman, S.; Chen, W.; Persson, K.A.; Ceder, G. Nucleation of metastable aragonite $CaCO_3$ in seawater. *Proc. Natl. Acad. Sci. USA* **2015**, *112*, 3199–3204. [CrossRef]
35. Chave, K.E. A Solid Solution between Calcite and Dolomite. *J. Geol.* **1952**, *60*, 190–192. [CrossRef]
36. Wasylenki, L.E.; Dove, P.M.; Wilson, D.S.; De Yoreo, J.J. Nanoscale effects of strontium on calcite growth: An in situ AFM study in the absence of vital effects. *Geochim. Cosmochim. Acta* **2005**, *69*, 3017–3027. [CrossRef]
37. Astilleros, J.; Fernández-Díaz, L.; Putnis, A. The role of magnesium in the growth of calcite: An AFM study. *Chem. Geol.* **2010**, *271*, 52–58. [CrossRef]
38. Hashim, M.S.; Kaczmarek, S.E. The transformation of aragonite to calcite in the presence of magnesium: Implications for marine diagenesis. *Earth Planet. Sci. Lett.* **2021**, *574*, 117166. [CrossRef]
39. Mills, J.V.; Barnhart, H.A.; DePaolo, D.J.; Lammers, L.N. New insights into Mn^{2+} and Mg^{2+} inhibition of calcite growth. *Geochim. Cosmochim. Acta* **2022**, *334*, 338–367. [CrossRef]
40. Walter, L.M.; Morse, J.W. The dissolution kinetics of shallow marine carbonates in seawater: A laboratory study. *Geochim. Cosmochim. Acta* **1985**, *49*, 1503–1513. [CrossRef]
41. Astilleros, J.; Pina, C.; Fernández-Díaz, L.; Putnis, A. Metastable phenomena on calcite 101-4 surfaces growing from Sr^{2+}–Ca^{2+}–CO_3^{2+} aqueous solutions. *Chem. Geol.* **2003**, *193*, 93–107. [CrossRef]
42. Weiss, I.M.; Tuross, N.; Addadi, L.; Weiner, S. Mollusc larval shell formation: Amorphous calcium carbonate is a precursor phase for aragonite. *J. Exp. Zool.* **2002**, *293*, 478–491. [CrossRef]
43. Huang, J.; Liu, C.; Xie, L.; Zhang, R. Amorphous calcium carbonate: A precursor phase for aragonite in shell disease of the pearl oyster. *Biochem. Biophys. Res. Commun.* **2018**, *497*, 102–107. [CrossRef]

44. Grünewald, T.A.; Checchia, S.; Dicko, H.; Le Moullac, G.; Sham Koua, M.; Vidal-Dupiol, J.; Duboisset, J.; Nouet, J.; Grauby, O.; Di Michiel, M.; et al. Structure of an amorphous calcium carbonate phase involved in the formation of Pinctada margaritifera shells. *Proc. Natl. Acad. Sci. USA* **2022**, *119*, e2212616119. [CrossRef]
45. Fitzer, S.C.; Chung, P.; Maccherozzi, F.; Dhesi, S.S.; Kamenos, N.A.; Phoenix, V.R.; Cusack, M. Biomineral shell formation under ocean acidification: A shift from order to chaos. *Sci. Rep.* **2016**, *6*, 21076. [CrossRef]
46. Ramesh, K.; Hu, M.Y.; Thomsen, J.; Bleich, M.; Melzner, F. Mussel larvae modify calcifying fluid carbonate chemistry to promote calcification. *Nat. Commun.* **2017**, *8*, 1709. [CrossRef] [PubMed]
47. Simmer, R.A.; Jansen, E.J.; Patterson, K.J.; Schnoor, J.L. Climate Change and the Sea: A Major Disruption in Steady State and the Master Variables. *ACS Environ. Au* **2023**, *3*, 195–208. [CrossRef]
48. Castellan, G.; Angeletti, L.; Canese, S.; Mazzoli, C.; Montagna, P.; Schiaparelli, S.; Taviani, M. Visual Imaging of Benthic Carbonate-Mixed Factories in the Ross Sea Region Marine Protected Area, Antarctica. *Minerals* **2021**, *11*, 833. [CrossRef]
49. Cubillas, P.; Köhler, S.; Prieto, M.; Chaïrat, C.; Oelkers, E.H. Experimental determination of the dissolution rates of calcite, aragonite, and bivalves. *Chem. Geol.* **2005**, 216, 59–77. [CrossRef]
50. Hadjittofis, E.; Vargas, S.M.; Litster, J.D.; Sedransk Campbell, K.L. The role of surface energy in the apparent solubility of two different calcite crystal habits. *Proc. R. Soc. A* **2021**, *477*, 20210200. [CrossRef] [PubMed]
51. Bychkov, A.Y.; Bénézeth, P.; Pokrovsky, O.; Shvarov, Y.V.; Castillo, A.; Schott, J. Experimental determination of calcite solubility and the stability of aqueous Ca–and Na–carbonate and–bicarbonate complexes at 100–160 °C and 1–50 bar pCO_2 using in situ pH measurements. *Geochim. Cosmochim. Acta* **2020**, *290*, 352–365. [CrossRef]